Results in Physics 34 (2022) 105209

Contents lists available at ScienceDirect

Results in Physics

journal homepage: www.elsevier.com/locate/rinp

Photoacoustic response optimization of gold nanorods in the near-infrared region

Jian-Ping Sun [a,b], Ya-Tao Ren [a,b,c,*], Kai Wei [a,b], Ming-Jian He [a,b], Bao-Hai Gao [a,b], Hong Qi [a,b,*]

[a] School of Energy Science and Engineering, Harbin Institute of Technology, Harbin 150001, China
[b] Key Laboratory of Aerospace Thermophysics, Ministry of Industry and Information Technology, Harbin 150001, China
[c] Faculty of Engineering, University of Nottingham, University Park, Nottingham NG7 2RD, UK

ARTICLE INFO

Keywords:
Photoacoustic
Gold nanorods
Localized surface plasmon resonance
Size optimization

ABSTRACT

Photoacoustic imaging (PAI) combines the advantage of optical and ultrasonic imaging, which has a high signal-to-noise ratio, and spatial resolution. To further improve the performance of PAI, gold nanorods can be utilized as exogenous contrast agents, and their size can be controlled. The size change of gold nanorods will change their absorption and heat transfer characteristics, and then affect their photoacoustic characteristics. Therefore, in the present work, the influences of absorption characteristics (absorption cross section and volume absorption coefficient) and heat transfer characteristics (specific surface area) of gold nanorods on photoacoustic response are studied by FDTD (FDTD Solutions, Lumerical) and FEM (Comsol Multiphysics). Results show that the increase of specific surface area will enhance the thermal coupling between gold nanorods and water, so as to improve the heat transfer and produce different photothermal responses without significantly affecting the photoacoustic quantum yield (As the specific surface area increases by about 10 times, the temperature increases by about 12 times, while the photoacoustic quantum yield increases by about 24%). On the contrary, absorption characteristics are decisive factors for both photothermal and photoacoustic responses. Therefore, in terms of improving photoacoustic quantum yield, when the size of gold nanorods changes, more attention should be paid to the improvement of the absorption characteristics rather than the specific surface area. In addition, increasing the specific surface area can significantly improve the photostability of gold nanorods, which is very important for practical applications.

Introduction

Photoacoustic imaging (PAI) combines the advantages of optical imaging and ultrasonic imaging, which has a high signal-to-noise ratio, and spatial resolution. As a non-ionizing and non-invasive imaging method, it has great potential in biomedical imaging [1]. The generation of a photoacoustic (PA) signal has four different mechanisms: thermal expansion, vaporization, photochemical reaction, and optical breakdown depending on the laser intensity and other factors [2]. For photoacoustic imaging of biological tissues, the only safe method is the photoacoustic effect based on thermal expansion [2]. However, in terms of photoacoustic conversion efficiency, the photoacoustic effect based on the medium's thermal expansion mechanism is relatively weak, causing photoacoustic imaging based on an endogenous contrast agent to have some defects such as low sensitivity and insufficient contrast [3]. Different exogenous contrast agents have been developed to overcome these defects, including small chromophores, fluorescent proteins, carbon nanoparticles, semiconductors, and plasmonic nanomaterials [4,5]. Plasmonic nanomaterials, represented by gold nanoparticles (AuNPs), have been investigated due to their unique advantages. First, AuNPs have strong light absorption/scattering characteristics due to the localized surface plasmon resonance (LSPR) effect [6,7]. Second, because of their simple fabrication, various synthesis methods, and various forms, such as rods, cages, and shells, they have numerous choices in practical application [8,9]. Most importantly, their stable surface chemistry makes them biologically inert [10] and easy to bind with targeted ligands [11]. Therefore, gold nanoparticles as contrast agents have been widely utilized in photoacoustic imaging [12–16].

With the successful application of photoacoustic imaging of biological tissues with gold nanoparticles as the contrast agent, research on the photoacoustic response mechanism and influencing factors of gold nanoparticles has garnered a great deal of attention. Due to the

* Corresponding authors at: School of Energy Science and Engineering, Harbin Institute of Technology, Harbin 150001, China.
E-mail addresses: renyt@hit.edu.cn (Y.-T. Ren), qihong@hit.edu.cn (H. Qi).

https://doi.org/10.1016/j.rinp.2022.105209
Received 19 October 2021; Received in revised form 24 December 2021; Accepted 6 January 2022
Available online 12 January 2022

simplicity of their structure, research on the mechanism of the photoacoustic effect of gold nanoparticles is mostly focused on spherical nanoparticles, and some important results have been obtained. Chen et al. [17] theoretically calculated the photoacoustic signal of the ideal model of gold nanospheres in water. Combined with the experimental verification, it was proved that the photoacoustic signal generated by the AuNPs solutions mainly came from the water instead of the AuNPs. Moreover, they found that the photoacoustic signal generated by AuNPs is responsible for less than 1% of the detected signal strength. Yu et al. [18] systematically studied the effects of geometry, surrounding media, laser intensity, and laser pulse width on the photoacoustic response of SiO_2-coated gold nanoshell in the near-infrared band by using the finite element method, and optimized the structure of the gold nanoshell. Shahbazi et al. [19] obtained the analytical solution for the photoacoustic response of core–shell nanospheres. On this basis, the effects of interface thermal resistance and the pulse laser waveform on photoacoustic signals of nanospheres were studied, and the proportion of photoacoustic signals generated by the shell and water layer was investigated. It was demonstrated that the water layer radius that can generate photoacoustic signals is twice that of the spherical radius.

While the photoacoustic effect of gold nanospheres has been investigated thoroughly, the LSPR wavelength of gold nanospheres is generally located in the visible region [20–25], which has a relatively small penetration depth in biological tissue. In the near-infrared region, the absorption rate of biological tissue is lower, allowing the use of larger laser fluence, which is conducive to the application of photoacoustic imaging in deep biological tissue. Therefore, other morphologies of gold nanoparticles that can show high absorption characteristics in the near-infrared region have attracted much attention. Compared with other morphologies, nanorods have more potential applications in the near-infrared region due to their advantages of simple synthesis and tunable surface plasmon resonances [26]. The photoacoustic effect of gold nanorods has been studied. Chen et al. [27] proposed a synthesis method for miniature gold nanorods, which proved that the properties of miniature gold nanorods were theoretically and experimentally more effective compared to regular-sized gold nanorods (AuNRs). Shi et al. [28] studied the quantitative relationship between the photoacoustic conversion efficiency and the size of gold nanospheres and nanorods. It was found that the optimal sizes of gold nanospheres and gold nanorods were 60 nm in diameter and 56 nm × 16 nm in length and width respectively. However, the optimization of gold nanorods is carried out under the condition of a fixed aspect ratio, and when the aspect ratio changes, the optimized results are no longer applicable. Through experimental research, Oscar et al. [29] compared the performance of four sizes of gold nanorods in photoacoustic conversion efficiency, melting threshold, and cytotoxicity. It was found that AuNRs with $r =$ 40 nm and $r = 50$ nm (r is the gold nanorod radial length) produced the strongest signal for the same number of particles, but had the strongest toxicity. On the contrary, the photoacoustic conversion efficiency of AuNRs with $r = 10$ nm was the highest under the same total mass.

The purpose of studying the mechanism of photoacoustic response of gold nanorods is to have a deeper insight of physical processes, so as to optimize the structure of gold nanorods with better photoacoustic performance. However, researches on the photoacoustic response mechanism and structure optimization of gold nanorods are still insufficient. The size change of gold nanorods will change the absorption and heat transfer characteristics of gold nanorods at the same time, but there is a lack of quantitative research on the influence of the two on the photothermal response and photoacoustic response of gold nanorods. In addition, for the size optimization of gold nanorods, in the current research, the size range of gold nanorods studied is very small, such as fixed aspect ratio [28] or qualitative research on only four commercially available gold nanorod sizes [29]. There is a lack of research on the size optimization of gold nanorods with the best photoacoustic response considering the absorption and heat transfer characteristics under a specific near-infrared spectrum.

In this work, finite difference time domain (FDTD, Lumerical) and finite element method (FEM, COMSOL) are used to study the photoacoustic effect of AuNRs in an aqueous solution. The effects of incident laser wavelength (i.e. absorption characteristics) and specific surface area (i.e. heat transfer characteristics) of gold nanorods on photothermal response and photoacoustic response of a single gold nanorod are quantitatively analyzed through numerical simulation. Then, the relationship between the photoacoustic quantum yield of single gold nanorod and the photoacoustic quantum yield of macro gold nanorod solution is established. Furthermore, the sizes of gold nanorod at 808 nm, 895 nm and 1064 nm in the near-infrared region are optimized to achieve the highest photoacoustic signal of the macro solution. Finally, for the optimized size of gold nanorods, the suggestions to ensure the thermal stability are given by calculating the critical laser fluence that leads to the phase change of water around AuNRs.

Photoacoustic response model of the AuNP

Physical process

The LSPR effect of the gold nanoparticle in an aqueous solution occurs due to laser irradiation. The gold nanoparticle scatters part of the pulse laser energy, and the other part is absorbed and converted into thermal energy, which leads to a rapid temperature rise of the gold nanoparticle within a short period. The temperature difference between the gold nanoparticle and the surrounding water induces a nanosecond heat transfer process, causing a rapid temperature change of the surrounding water. As a result, thermal expansion occurs in the surrounding water, which means that the water will produce elastic stress and strain, resulting in pressure changes. The pressure change will cause acoustic wave-propagation, which can be detected as a real-time PA signal. The whole physical process is shown in Fig. 1.

PA response model

When the gold nanoparticle is illuminated by a linearly polarized plane wave with frequency ω, the electric field $\mathbf{E}$ and magnetic field intensities $\mathbf{H}$ can be calculated by the Maxwell's curl equations[30]. Then, the absorption cross section C_{abs}, scattering cross section C_{sca}, and extinction cross section C_{ext} of the gold nanoparticle respectively can be calculated by [31]:

$$C_{\text{abs}}(\omega) = \frac{P_{\text{abs}}(\omega)}{I_0(\omega)} \tag{1}$$

$$C_{\text{sca}}(\omega) = \frac{P_{\text{sca}}(\omega)}{I_0(\omega)} \tag{2}$$

$$C_{\text{ext}}(\omega) = C_{\text{abs}}(\omega) + C_{\text{sca}}(\omega) \tag{3}$$

where I_0 is the incident laser fluence, and P is the total energy absorbed or scattered by nanoparticles. The expression of P is complex, which can be seen in the literature [32].

The absorbed electromagnetic energy is converted into thermal energy of the gold nanoparticle, which can be calculated as the resistive heating q_{r} [33]:

$$q_{\text{r}} = I_0 C_{\text{abs}} / V \tag{4}$$

where V is the volume of nanoparticles.

The temperature of the gold nanoparticle rises rapidly because of resistance heating. When illuminated by a nanosecond pulsed laser, the electronic temperature of the electronic gas is equal to the temperature of the lattice (phonons) [34], which means that the heat transfer and temperature distribution in the gold nanoparticle and surrounding water can be calculated by the transient Fourier heat conduction equation [35]:

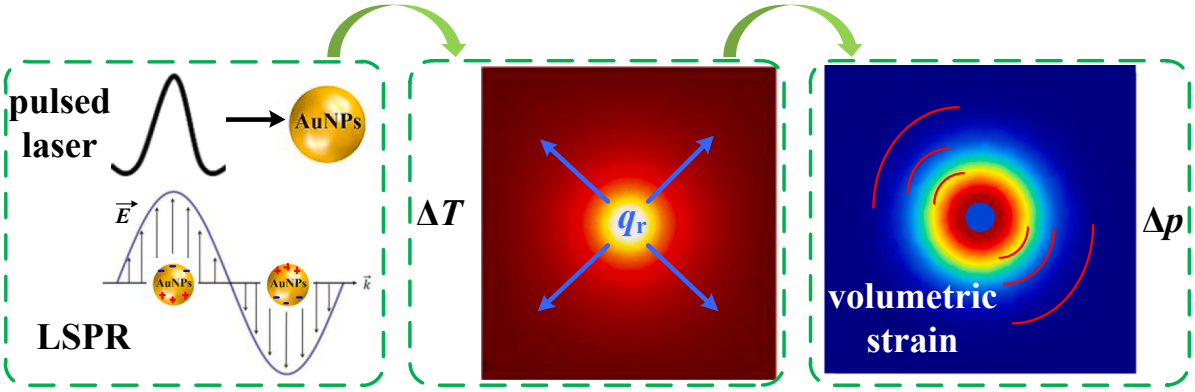

Fig. 1. Schematic of physical process of photoacoustic effect of the gold nanoparticle.

$$\rho c\frac{\partial T}{\partial t} = \nabla\kappa\nabla T + q_t f(t) \tag{5}$$

whereρ, c, κ, and T are the density, heat capacity, thermal conductivity, and temperature, respectively. Here, the function, $f(t)$, represents the temporal Gaussian-shaped laser pulse, which is defined as:

$$f(t) = \frac{1}{\delta\sqrt{2\pi}}exp\left[-\frac{(t-t_0)^2}{2\delta^2}\right] \tag{6}$$

where t is the time, t_0 is the time position of the center of the peak, and $\delta = t_w/\left(2\sqrt{2ln2}\right)$ is the standard deviation. Here, t_w is the full width at half-maximum of the Gaussian profile (i.e. the pulse duration of the pulsed laser).

At the interface of different material surfaces, there is interfacial thermal resistance, which makes the temperature distribution on both sides of the interface discontinuous. The boundary conditions at the interface meet the following formula [36]:

$$(T_1 - T_2)G_{12} = -\kappa_2\nabla T\cdot\boldsymbol{n} \tag{7}$$

where subscripts "1" and "2" respectively represent the media on both sides of the interface, G is the thermal conductivity of the interface, and **n** represents the normal direction of the interface.

Linear thermal expansion occurs due to an increased temperature in the gold nanoparticle and the surrounding water. The corresponding stress–strain tensor can be calculated by the Duhamel-Hookes equation [37]:

$$\boldsymbol{s} = \boldsymbol{C} : (\boldsymbol{\varepsilon} - \alpha(T - T_0)) \tag{8}$$

where **s** is the total stress tensor, **C** is the fourth-order elasticity tensor related to shear and bulk modulus, "**:**" is defined as the double-dot product, ε is the total strain tensor, αis the thermal expansion coefficient, and T_0 is the reference temperature.

The convection of fluid in the whole process of thermal expansion is ignored. Therefore, the water medium around the gold nanoparticle can be regarded as a solid, and its elastic properties can be represented by shear and bulk moduli [38].

The thermal expansion-induced total displacement **u** can be calculated from the total stress tensor **s** through the following equation [37]:

$$\nabla\boldsymbol{s} = \rho\frac{\partial^2\boldsymbol{u}}{\partial t^2} \tag{9}$$

The acoustic pressure change can be calculated from the thermal expansion-induced total displacement **u** by [37]:

$$\boldsymbol{n}_2\cdot\left(\frac{1}{\rho}\nabla p_t\right) = -\boldsymbol{n}_2\cdot\frac{\partial^2\boldsymbol{u}}{\partial t^2} \tag{10}$$

where $\mathbf{n}_2$ is the outward normal to the boundary, and $p_t = p + p_b$ is the total acoustic pressure. Here, p is the PA signal and p_b is the ambient pressure.

The propagation and pressure distribution of the PA signal in the surrounding medium can be obtained by solving the following acoustic wave equation [18]:

$$\frac{1}{\rho v_s^2}\frac{\partial^2 p_t}{\partial t^2} - \nabla\left[\frac{1}{\rho}(\nabla p_t)\right] = 0 \tag{11}$$

where v_s is the speed of sound.

Method and verification

In this work, the absorption cross section of gold nanorods is calculated by finite difference time domain (FDTD, Lumerical), and the photothermal and photoacoustic responses of gold nanorods are calculated by finite element method (FEM, COMSOL).

When calculating the absorption cross section of gold nanorods, a single gold nanorod is irradiated by linearly polarized light in water, and the perfectly matched layer is used as the external boundary condition to eliminate the influence of reflected electromagnetic wave. In order to verify the accuracy of the calculation, the convergence experiment is carried out, which has set an error limit of 10^{-5}. In the calculation, there are dense grids near the gold nanorods, and the grid size is related to the size of the gold nanorods. Gold nanorods are composed of hemispheres at both ends and cylinders in the middle. The radius of hemispheres and cylinders is r, the height of cylinders is H, the length of gold nanorods is $L = H + 2r$, and the aspect ratio is AR $= L/2r$. The grid size shall meet radial step $\Delta r = 2r/15$, axial step $\Delta h = H/40$, and the maximum value of Δr and Δh shall not exceed 1 nm. When the linearly polarized light is along the axial direction of the gold nanorod, it is compared with the absorption cross section of the gold nanorod calculated by the finite element method in the literature [39]. As shown in Fig. 3 (a), the results are in good agreement with the literature.

The coupled partial differential equations of transient heat transfer equation, transient structural mechanics equation and transient sound propagation method are solved by finite element method (FEM, COMSOL), as shown in Fig. 2. Fourier heat conduction equation and generalized Hooke's law equation are solved in Domain-I, and the coupling variable is temperature T. In the heat transfer equation, the heat source is gold nanorods. It is assumed that the position of the yellow dotted line is the boundary (called "Boundary") and is set as an isothermal wall, equal to the initial temperature. In the structural mechanics equation, both gold nanorods and water are linear thermal expansion media, and others are the default settings. The sound propagation equation is solved in Domain-II, and the boundary condition is spherical wave radiation at the outermost boundary to reduce the influence of reflected sound waves. The coupling variables of structural mechanics equation and

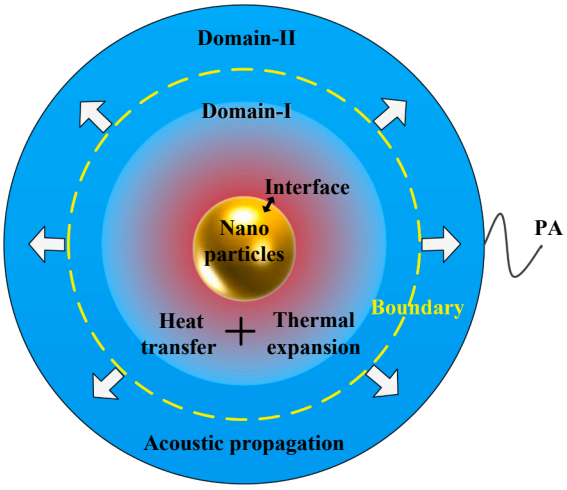

Fig. 2. Schematic of the PA response model of the gold nanoparticle.

sound propagation equation are displacement **u** and pressure p, which are coupled at Boundary by Eq. (10). In the calculation, the transient solver is used to solve the above three coupled partial differential equations at the same time. In order to reduce the use of computer memory, the separate solver is used, and a relative error limit is set to 10^{-4} and the time step is 0.2 ns. The grid size is related to the size of gold nanorods. The maximum grid size of gold nanorods is (r/2–1) nm, the minimum grid size of other regions is 0.1 nm, the maximum grid size is 250 nm, and the maximum grid growth rate is 1.45. The total number of grids is between 16,000 and 23000, depending on the size of gold nanorods. Domain-I and Domain-II are spheres with a radius of (r + 700) nm and (r + 1000) nm, respectively. In order to verify the accuracy of the heat transfer model, the temperature distribution of gold nanospheres with a radius of 30 nm under the irradiation of pulsed laser with a pulse duration of 10 ns and a wavelength of 532 nm is calculated and compared with the results in the literature [19]. As shown in Fig. 3(b) and Fig. 3(c), the results are in good agreement with the literature. Ref. [40] gives the time profile distribution model $p(r,t) = -p_0\frac{\sqrt{2e}v_s}{r_0}\left(t-\frac{r}{v_s}\right)exp\left\{-\left[\frac{v_s}{r}\left(t-\frac{r}{v}\right)\right]^2\right\}$ of photoacoustic pressure of spherical objects excited by Gaussian pulses. The photoacoustic pressure results of gold nanospheres calculated in this work are compared with them, as shown in Fig. 3 (d). It can be seen that the results are in good agreement with the literature.

Results and discussion

In the application of biomedical photoacoustic imaging, the photoacoustic effect of gold nanorods is a derivative effect of thermal expansion, which originates from the photothermal conversion of gold nanorods and the heat transfer process between gold nanorods and the

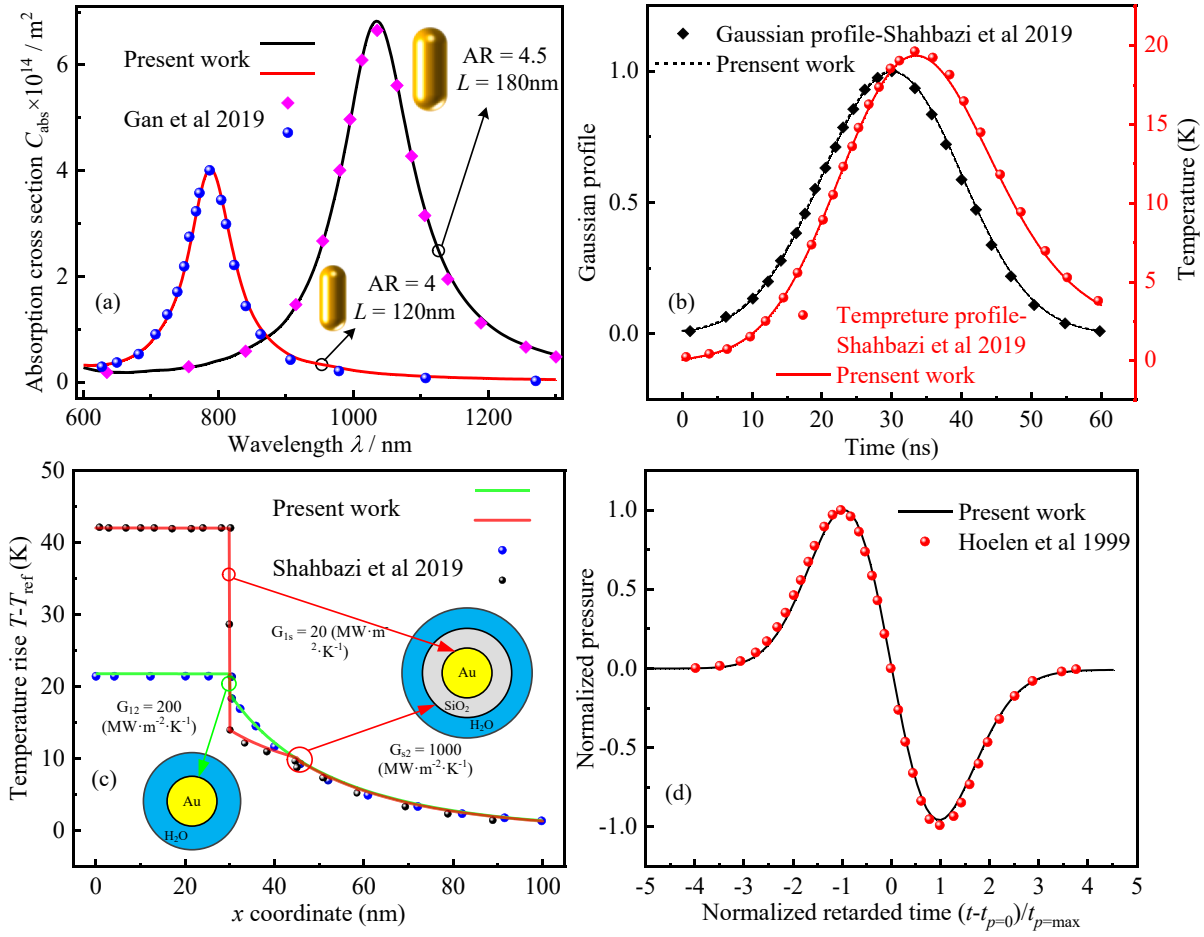

Fig. 3. Validation of present model: (a) Absorption cross section distribution of gold nanorods. The polarization direction of linearly polarized light is along the axial direction of gold nanorods. (b) Gaussian profile of pulsed laser and temperature profile distribution of the gold nanosphere. The radius of gold nanosphere is 30 nm and the pulse duration of pulsed laser is 10 ns. (c) Radial temperature distribution of the gold nanosphere. The radius of gold nanosphere is 30 nm, the thickness of SiO_2 shell is 15 nm, and the time is 30 ns (when the pulse laser intensity is the maximum). (d) Temporal profile of the normalized PA pulse generated by a gold nanosphere heated by Gaussian pulse.

surrounding aqueous medium. The former is affected by nanosecond pulsed laser and the absorption cross section of gold nanorods, and the latter is mainly determined by the heat transfer area between gold nanorods and water (defined here as the specific surface area, that is, the ratio of surface area to volume of gold nanorods) and the interfacial thermal resistance (Kapitza resistance) between gold and water. When the size of gold nanorods is changed, the absorption cross-section distribution and heat transfer area to water are changed, resulting in the change of photoacoustic response. Therefore, the effects of absorption cross section and specific surface area of gold nanorods on their photothermal response and photoacoustic response are analyzed separately. Furthermore, the size of gold nanorods used in near-infrared region is optimized to maximize the photoacoustic quantum yield of gold nanorods at corresponding wavelengths.

The physical parameters of Au and H_2O are shown in Table 1.

Laser wavelength

The absorption cross sections of four different sizes of gold nanorods were calculated by FDTD, as shown in Fig. 4(a). Because the axial and radial directions of gold nanorods are asymmetric, gold nanorods will show different absorption cross-section distribution when laser irradiates gold nanorods with different polarization directions. Meanwhile, the nanorods are likely to have a vast arrangement of orientations in solution, which is random. Therefore, it is necessary to average the absorption cross section distribution in each polarization direction of gold nanorods. However, this is time-consuming and requires a lot of computing resources. Previous studies have shown that for gold nanorods, the average results in each direction can be replaced by the average absorption cross sections in both radial and axial directions [41]. Therefore, the absorption cross section calculated in this work is the average of radial and axial polarization directions. As can be seen in Fig. 4(a), gold nanorods have absorption peaks near 530 nm and near-infrared region respectively, while the second absorption peak of gold nanorods significantly redshifts when the aspect ratio increases. The absorption peak originates from the LSPR of gold nanorods. The latter will happen under two conditions. Firstly, the size range of gold nanorods is in the nanometer level, which is equivalent to the average free path of free electrons on the surface. Secondly, the external laser with a specific frequency irradiates the gold nanorods to make the free electrons on the surface of gold nanorods resonate with photoelectric magnetic wave [42], resulting in the increase of local electric field and the conversion of light energy into heat energy through Joule heat. The resonance frequency strongly depends on the relative relationship between the average electron free path and the size of gold nanorods. Due to the huge size difference between radial and axial direction, there are two absorption peaks corresponding to radial and axial direction respectively. Therefore, the absorption cross-section distribution of gold nanorods can be adjusted by changing the aspect ratio. Moreover, Fig. 4 (a) shows that the maximum absorption cross section of gold nanorods decreases significantly with the decrease of length and the increase of aspect ratio, while the volume of gold nanorods decreases significantly with the decrease of length and the increase of aspect ratio. They show a certain positive correlation, which may be due to the significant decrease of polarizability of gold nanorods with the decrease of the volume. In Ref. [43], it is considered that the absorption cross section of gold nanoparticles is directly proportional to the volume.

Furthermore, taking the gold nanorod with AR = 3 and $L = 90$ nm as an example, the photothermal response of gold nanorods irradiated by nanosecond pulsed laser with different wavelengths was studied, as shown in Fig. 4(b). It shows the temperature distribution at the central origin (the center of the gold nanorod). Since the thermal diffusion coefficient of gold is three orders of magnitude higher than that of water (the thermal diffusion coefficient of gold is 1.29×10^{-4} $m^2 \cdot s^{-1}$ and that of water is 1.4×10^{-7} $m^2 \cdot s^{-1}$), the temperature distribution in gold nanorods can be considered to be uniform, which means that the results in the figure can represent the temperature distribution of gold nanorods. Gold nanorods have different absorption cross sections at different laser wavelengths. Larger absorption cross section means that gold nanorods have stronger light absorption ability, resulting in higher temperature of gold nanorods with larger absorption cross section at each time. The time profile of gold nanorod temperature is mainly determined by the time profile of pulsed laser. Therefore, each curve in Fig. 4(b) shows the same trand. The inset on the left in Fig. 4(b) shows the change of axial temperature spatial distribution of gold nanorods and surrounding aqueous medium with time when the laser wavelength is 774 nm. It can be seen that the heat transfer process of gold nanorods is at the nano level in space and nanosecond level in time. This means that the influence of the heat transfer process of gold nanorods on the macro biological tissue can be ignored, even if the heat transfer process produces a temperature rise of hundreds of Kelvin (no phase change in aqueous medium), which ensures the biological safety of the biological tissue photoacoustic imaging technology using gold nanorods as photoacoustic contrast agent.

The photoacoustic effect of gold nanorods originates from the pressure change caused by the thermal expansion of gold nanorods and surrounding water medium, resulting in detectable photoacoustic signals. The thermal expansion coefficient of water is about 5 times that of gold (see Table 1), and the area of thermal expansion of water is also larger than that of gold nanorods. Therefore, it can be considered that the photoacoustic response of gold nanorods is mainly contributed by the temperature changing water around gold nanorods. Chen et al. [17] have proved this view theoretically, that is, for the photoacoustic response of gold nanospheres, the photoacoustic pressure generated by gold nanospheres accounts for less than 1% of the total photoacoustic pressure. Therefore, it is necessary to study the temperature rise change of the water medium around different gold nanorods under different laser wavelengths (in this work, the effect of laser wavelength is essentially the effect of the absorption cross section of gold nanorods under different wavelengths, so it will be directly expressed by the absorption cross section of gold nanorods), as shown in Fig. 4(c). It can be seen that for gold nanorods of different sizes, under the same pulse laser fluence, the maximum temperature rise of water medium around gold nanorods is directly proportional to the absorption cross section of gold nanorods. However, for different sizes of gold nanorods, the slope of C_{abs}-ΔT_{water} curve is different. The gold nanorods have larger C_{abs}-ΔT_{water} curve slope, which is equivalent to the same increase in absorption cross section, the water medium around the gold nanorods can have higher temperature rise, which means that the gold nanorods have higher heat transfer efficiency to the surrounding water medium. In Fig. 4(c), the aspect ratio of the four kinds of gold nanorods increases

Table 1
Physical parameters used for PA model.

Parameters	Symbol	Value
Dielectric function of gold	ε_{Au}	Johnson and Christy [64]
Refractive index of water	n_{H_2O}	1.33
Density of gold	ρ_{Au}	19300 kg/m^3
Density of water	ρ_{H_2O}	1000 kg/m^3
Thermal conductivity of gold	κ_{Au}	318 W/m/K
Thermal conductivity of water	κ_{H_2O}	0.6 W/m/K
Shear modulus of gold	Y_{Au}	75×10^9N/m^2
Poisson's ratio of gold	ν_{Au}	0.42
Shear modulus of water	G_{H_2O}	0 N/m^2
Bulk modulus of water	K_{H_2O}	2.15×10^9 N/m^2
Linear expansion coefficient of gold	α_{Au}	0.14×10^{-6} 1/K
Linear expansion coefficient of water	α_{H_2O}	70×10^{-6} 1/K
Heat capacity of gold	c_{Au}	129 J/kg/K
Heat capacity of water	c_{H_2O}	4200 J/kg/K
Sound velocity of water	$v_{s\_H_2O}$	1500 m/s

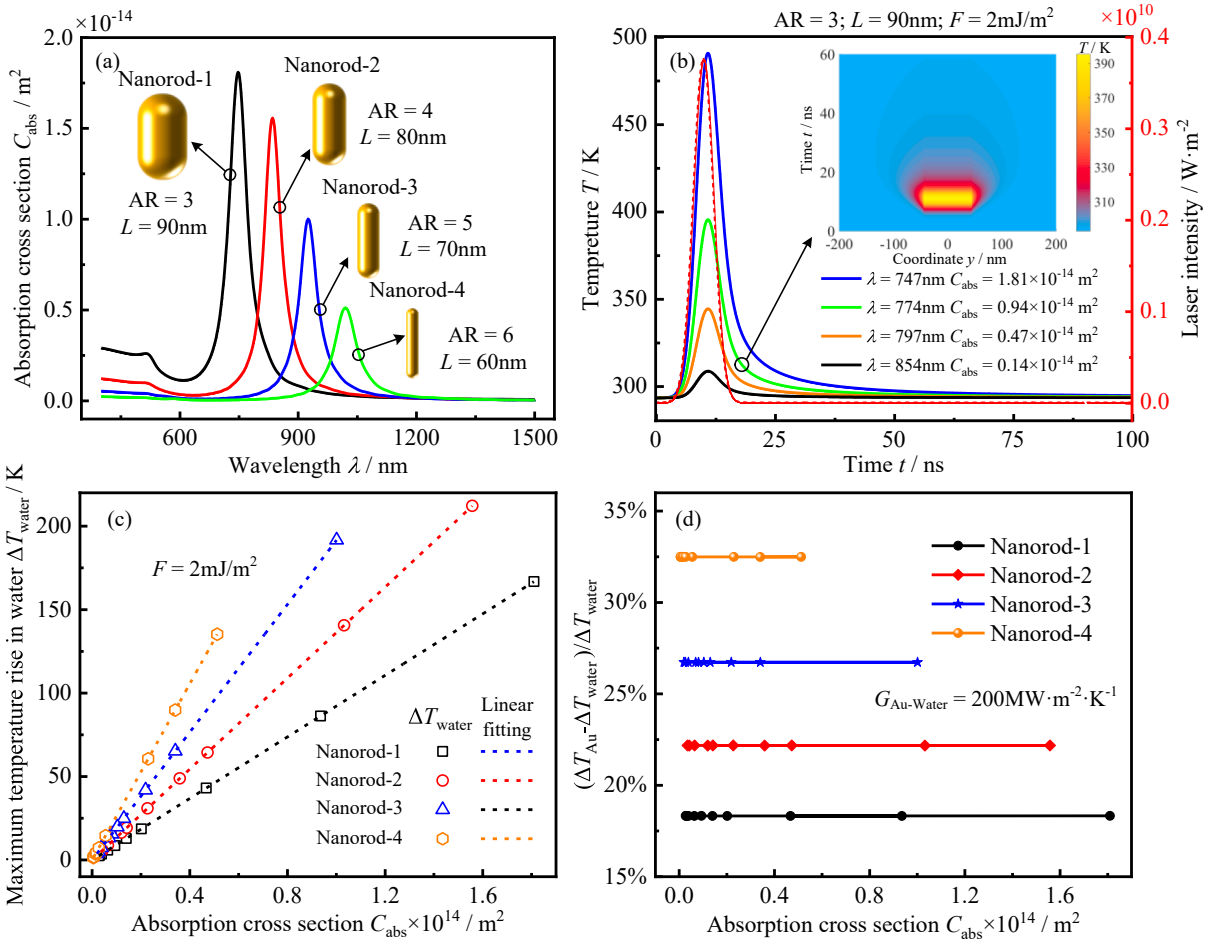

Fig. 4. Absorption characteristics and photothermal response of gold nanorods: (a) Absorption cross section distribution of four sizes of gold nanorods. The results are the radial and axial average of gold nanorods. (b) Temporal profile of the temperature at the center of gold nanorods at different wavelengths. The sizes of gold nanorods are AR = 3 and L = 90 nm, corresponding to Nanorod-1. The laser fluence is 2 mJ/m^2, the pulse duration is 5 ns, and the laser intensity distribution is the red dotted line in the figure (the later results are under the irradiation of this pulsed laser). The inset shows the axial temperature distribution of gold nanorods at a wavelength of 774 nm and a time step of 0.1 ns. (c) Variation of maximum temperature rise in water with absorption cross section of gold nanorods with different sizes. (d) The increasing ratio of the maximum temperature rise of gold nanorods to the maximum temperature rise in water varies with the absorption cross section. (For interpretation of the references to colour in this figure legend, the reader is referred to the web version of this article.)

and the length decreases in turn, so that the specific surface area of the gold nanorods increases gradually. Correspondingly, the slope of the C_{abs}-ΔT_{water} curve of the gold nanorods increases, which means that the heat transfer efficiency of the gold nanorods increases gradually.

There is a certain temperature drop at the interface between gold nanorods and aqueous medium due to the interfacial thermal resistance. The value of interfacial thermal resistance mainly depends on the properties of nanomaterials and surrounding media and the synthesis process of nano materials [44]. In this work, the value of interfacial thermal conductivity of Au-H_2O interface G = 200 MW•m^{-2}•k^{-1} is used for calculation to study the difference between the maximum temperature rise of gold nanorods and that of the surrounding aqueous medium at different laser wavelengths, as shown in Fig. 4(d). It can be seen that for a certain gold nanorod, the increase ratio of the maximum temperature rise of the gold nanorod relative to the aqueous medium is not affected by the laser wavelength. Combined with Fig. 4(c), it can be seen that the maximum temperature rise of the gold nanorod itself is also directly proportional to the absorption cross section, which also means that the larger the temperature rise of the gold nanorod, the larger the difference between the maximum temperature rise of the gold nanorod and water. Moreover, it is worth noting that the increase ratio of the maximum temperature rise of gold nanorods with different sizes relative to the aqueous medium is also different. The larger the specific surface area of gold nanorods, the greater the increase ratio, which means that when the specific surface area increases, the heat transfer efficiency of gold nanorods is improved, and meanwhile the influence of interfacial thermal resistance is also gradually enhanced. The interfacial thermal resistance will weaken the heat transfer enhancement caused by the increase of specific surface area, but it can not be completely eliminated.

The laser wavelength affects the photothermal response of gold nanorods, and then affects the photoacoustic response accordingly. Taking the gold nanorod with AR = 3 and L = 90 nm as an example, the photoacoustic response of gold nanorods at different wavelengths was studied, as shown in Fig. 5(a). It can be seen that the time profile of photoacoustic pressure of gold nanorods at different wavelengths is bipolar distribution, and the profile is highly similar to the second derivative of Gaussian pulse function to time, which means that the time profile of photoacoustic pressure of gold nanorods is mainly determined by Gaussian pulse function. However, due to the different absorption cross sections of gold nanorods at different laser wavelengths, there are significant differences in the value of photoacoustic pressure at each time. Obviously, the larger the absorption cross section of gold nanorods, the higher the temperature rise of gold nanorods and aqueous medium, and the stronger the photoacoustic pressure. Furthermore, in the application of biological photoacoustic imaging, attention is paid to the initial photoacoustic pressure amplitude of contrast agent and the

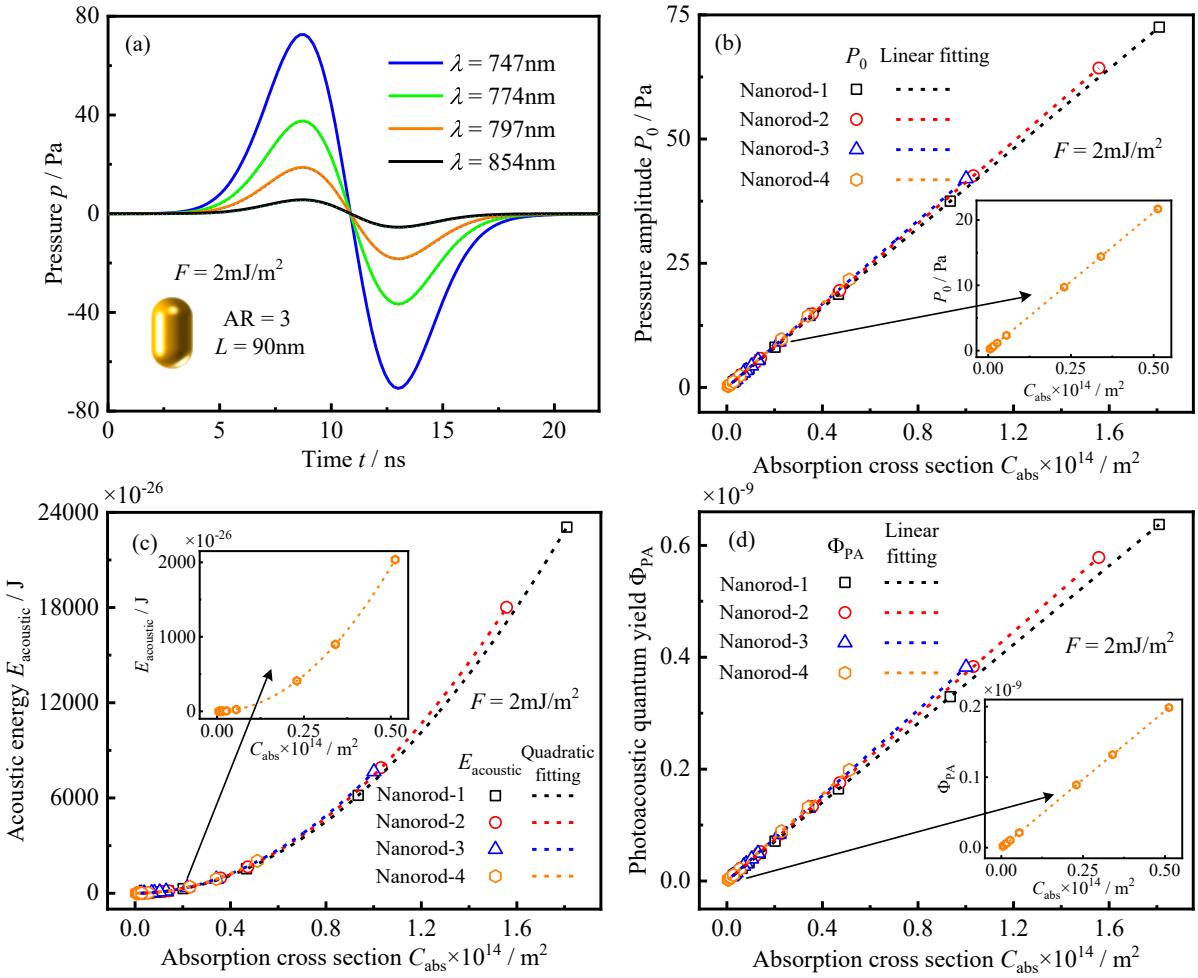

Fig. 5. Photoacoustic response of gold nanorods: (a) Temporal profile of photoacoustic pressure. (b) Variation of sound pressure amplitude with absorption cross section of gold nanorods. (c) Variation of acoustic energy with absorption cross section. (d) Variation of photoacoustic quantum yield with absorption cross section.

detected photoacoustic signal amplitude. Therefore, it is necessary to study the influence of laser wavelength on the photoacoustic pressure amplitude of gold nanorods, as shown in Fig. 5(b). It can be seen that for gold nanorods of different sizes, the pressure amplitude is directly proportional to the absorption cross section. Combined with Fig. 4(c) and Fig. 4(d), it can be inferred that the maximum temperature rise of gold nanorods, the maximum temperature rise of surrounding water, the pressure amplitude and the absorption cross section of gold nanorods are directly proportional to each other. When the pulse laser parameters are the same, according to Eq. (4), the absorption cross section is directly proportional to the heat generation of gold nanorods. Then, the photoacoustic pressure amplitude is actually proportional to the heat production of gold nanorods, which means that in addition to the absorption cross section of gold nanorods, the laser fluence is also proportional to the photoacoustic pressure of gold nanorods. This conclusion is consistent with the existing experimental results [27,45,46]. It is worth noting that in this work, the pulse energy is adjusted so as not to make the water phase change (i.e. the highest temperature of water is less than 550.15 K), which meets the non-invasive requirements of medical diagnosis.

In addition to the photoacoustic pressure amplitude, the photoacoustic quantum yield is also an important index to evaluate the photoacoustic properties of gold nanorods. The photoacoustic conversion efficiency of the AuNRs in an aqueous solution is defined as [27]:

$$\Phi_{PA} = \frac{E_{acoustic}}{E_{thermal}} = \frac{\iint p^2/R \mathrm{d}S\mathrm{d}t}{\int C_{abs} I \mathrm{d}t} \tag{12}$$

where, $E_{acoustic}$ is the sound energy of the photoacoustic system, $E_{thermal}$ is the thermal energy, $R = \rho_{H_2O} c_{H_2O}$ is the acoustic impedance of water, and S is the spherical surface with enough size containing the gold nanorods, so that the heat will not escape from the S plane.

The acoustic energy is directly related to the photoacoustic pressure time profile and is affected by the absorption cross section, as shown in Fig. 5(c). It can be seen that for gold nanorods of different sizes, the acoustic energy has a quadratic relationship with the absorption cross section, which can be proved from the analysis. From the definition of acoustic energy (see Eq. (12)), it can be known that acoustic energy has a quadratic relationship with photoacoustic pressure, and photoacoustic pressure is directly proportional to the absorption cross section. Therefore, the result in Fig. 5(c) is reasonable, and literature [27] also has the same conclusion. On this basis, the effect of absorption cross section of gold nanorods on photoacoustic quantum yield was quantitatively studied, as shown in Fig. 5(d). It can be seen that for gold nanorods of different sizes, the photoacoustic quantum yield is directly proportional to the absorption cross section, that is, directly proportional to the heat generation of gold nanorods, which means that the photoacoustic quantum yield of gold nanorods is affected not only by the properties of gold nanorods, but also by the parameters of pulsed laser. The higher heat production of gold nanorods can increase the temperature rise of gold nanorods and surrounding water medium, resulting in more significant thermal expansion effect and increasing the ratio of thermal energy to acoustic energy (that is the photoacoustic quantum yield). Furthermore, it is worth noting that for a single gold nanorod, the

photoacoustic quantum yield of gold nanorods is in the order of 10^{-9}, which is a very low value. It may be due to the fact that the photoacoustic effect is very small in time and space relative to the macro. In macro applications, the aqueous solution of gold nanorods usually contains hundreds of thousands of gold nanorods. The photoacoustic pressure of gold nanorods is directly proportional to the concentration of gold nanorods in the solution (we emphasize that when the overall concentration of nanoparticles is low, the statement is still true, and it has been proved experimentally[47,48]), which can significantly increase the photoacoustic quantum yield of the solution. However, the photoacoustic quantum yield of gold nanoparticles based on thermal expansion mechanism is still low [45], which is one of the limitations of photoacoustic imaging in biological applications.

Comparing Fig. 4(c) with Fig. 5(b), Fig. 5(c) and Fig. 5(d), it can be observed that there is a significant difference in the slope of C_{abs}-ΔT_{water} curve for gold nanorods of different sizes, while in terms of photoacoustic response, the curves of pressure amplitude, acoustic energy and photoacoustic quantum yield with absorption cross section are close to each other. This means that the change of heat transfer caused by the change of gold nanorod size will significantly affect its photothermal response, but it can not have as significant impact on the photoacoustic response as the photothermal response.

Heat transfer area (specific surface area)

When the size of the gold nanorods changes, their absorption cross section and specific surface area will also vary correspondingly. The essence of the absorption cross section affecting the photothermal and photoacoustic response of gold nanorods is to change the heat source of the system. To analyze the influence of specific surface area on photothermal and photoacoustic response of gold nanorods separately, it is necessary to eliminate the influence of heat source, that is, a single gold nanorod of different sizes has the same heat energy. It can be set that the thermal energy obtained by a single gold nanorod is 50 fJ (i.e. $E_{thermal} = F \bullet C_{abs} = 50$ fJ) and the pulse duration is the same as 5 ns. The photothermal response of a single gold nanorod with different sizes (The corresponding sizes of gold nanorods are shown in Table 2) was studied, and the variation curve of the maximum temperature rise of the aqueous medium around the gold nanorod with the specific surface area of the gold nanorod was obtained, as shown in Fig. 6(a). It can be seen that the maximum temperature rise of water is directly proportional to the specific surface area of gold nanorods. The larger specific surface area of gold nanorods means that the aspect ratio of gold nanorods is larger and the length of gold nanorods is smaller, that is, the volume of gold nanorods is smaller, and the heat generation power per unit volume of gold nanorods is larger and the temperature rise is higher when the same thermal energy is obtained. As a result, there is a larger temperature difference between the gold nanorods and the surrounding water medium, which makes the heat flux density of the whole heat transfer process higher and the heat transfer stronger. In Fig. 4(d), it is observed that the increase ratio of the maximum temperature rise of gold nanorods to the maximum temperature rise of water is also affected by the specific surface area of gold nanorods. Furthermore, the increase is directly proportional to the specific surface area of gold nanorods, as shown in Fig. 6(b). This means that by improving the synthesis technology of gold nanorods to reduce the interfacial thermal resistance between gold nanorods and surrounding media to improve the heat transfer efficiency, the effect of improvement is more significant for gold nanorods with larger aspect ratio and smaller length.

Table 2
Size of gold nanorods.

Aspect ratio AR	Length L / nm	Surface area S / nm^2	Volume V / nm^3	Surface to volume ratio S/V / nm^{-1}
2	100	15707.96	163,620	0.09600
3	90	8482.30	56,549	0.15000
4	80	5026.55	23,038	0.21818
5	70	3078.76	10,057	0.30612
6	60	1884.96	4450.6	0.42353
7	42	791.68	1131	0.70000
8	30	353.43	317.53	1.11300

Furthermore, the effects of the specific surface area of gold nanorods on the pressure amplitude and the photoacoustic quantum yield were studied, as shown in Fig. 6(c) and Fig. 6(d). It can be seen that the variation of pressure amplitude and photoacoustic quantum yield with specific surface area of gold nanorods is different from the effect of specific surface area on photothermal response, and there is no strict linear relationship. When the specific surface area is small (approximately on the left side of 0.5 nm^{-1} in the figure), the increase of its value will strongly increase the pressure and photoacoustic quantum yield. When the specific surface area is large (on the right side of 0.5 nm^{-1} in the figure), the change of specific surface area will not significantly change the photoacoustic effect of gold nanorods. This is closely related to the change in the volume of gold nanorods. It can be seen from Fig. 6(e) that the volume of gold nanorods changes sharply when the specific surface area is small and slowly when the specific surface area is large, which is consistent with the change of photoacoustic quantum yield. In addition, it is worth noting that our results are not consistent with those of Chen et al. [27]. Their results show that there is a linear relationship between the photoacoustic quantum yield and the specific surface area of gold nanorods, as shown in Fig. 6(f). We have a comparative discussion here. Different from our research, Chen et al. did not keep the heat source of gold nanorods fixed in the process of simulation. We believe that this is because it is difficult to ensure the effectiveness of optical density matching in the experimental process, and they ignore this factor in order to match the experimental results. This is reasonable in their research. However, it also means that the absorption properties will play a major role in the photoacoustic quantum yield of gold nanorods, as shown in Fig. 6(f). The volumetric absorption coefficient and photoacoustic quantum yield coincidentally have a linear relationship with the specific surface area. Combined with the results of Fig. 5(d), it is reasonable to believe that in the study of Chen et al., the linear relationship between photoacoustic quantum yield and specific surface area is dominated by absorption properties. Our calculation results are physically reasonable, that is, with the increase of the specific surface area, the photoacoustic quantum yield will reach a certain limit. If the photoacoustic quantum yield of gold nanorods is linear with the specific surface area, then when the object producing photoacoustic signal is a point heat source, the photoacoustic quantum yield will tend to infinity. Calasso et al.[49] provided an analytical expression of the photoacoustic pressure wave emitted by the "point absorber", $p(r,t) = E_{abs}\beta \frac{1}{c_p t_w^2} \frac{1}{4\pi r} \frac{df}{d\tau}\left(\tau = \frac{t - r/v_s}{t_w}\right)$. Obviously, the photoacoustic quantum yield of a point sound source is a finite value. Moreover, noting the results in Fig. 6(c) and Fig. 6(d), the specific surface area of gold nanorods increased from 0.096 nm^{-1} (corresponding to the size of gold nanorods AR = 2 and L = 100 nm) to 1.113 nm^{-1} (AR = 8 and L = 30 nm), which increased by 10.6 times, while the corresponding pressure amplitude and photoacoustic quantum yield increased by 0.13 times and 0.24 times respectively, with a difference of 1–2 orders of magnitude. This means that relative to the absorption cross section, the influence of specific surface area on the photoacoustic response of gold nanorods is more limited, that is, the absorption cross section will be the key factor dominating the photoacoustic effect of gold nanorods.

In the application of biological photoacoustic imaging, the number of gold nanorods contained in biological tissue is very large. When studying the effect of the specific surface area of gold nanorods on their photoacoustic response, the results of single gold nanorods may be different from those of macro gold nanorod solution. However, we still expect to obtain the photoacoustic response of the macro gold nanorod

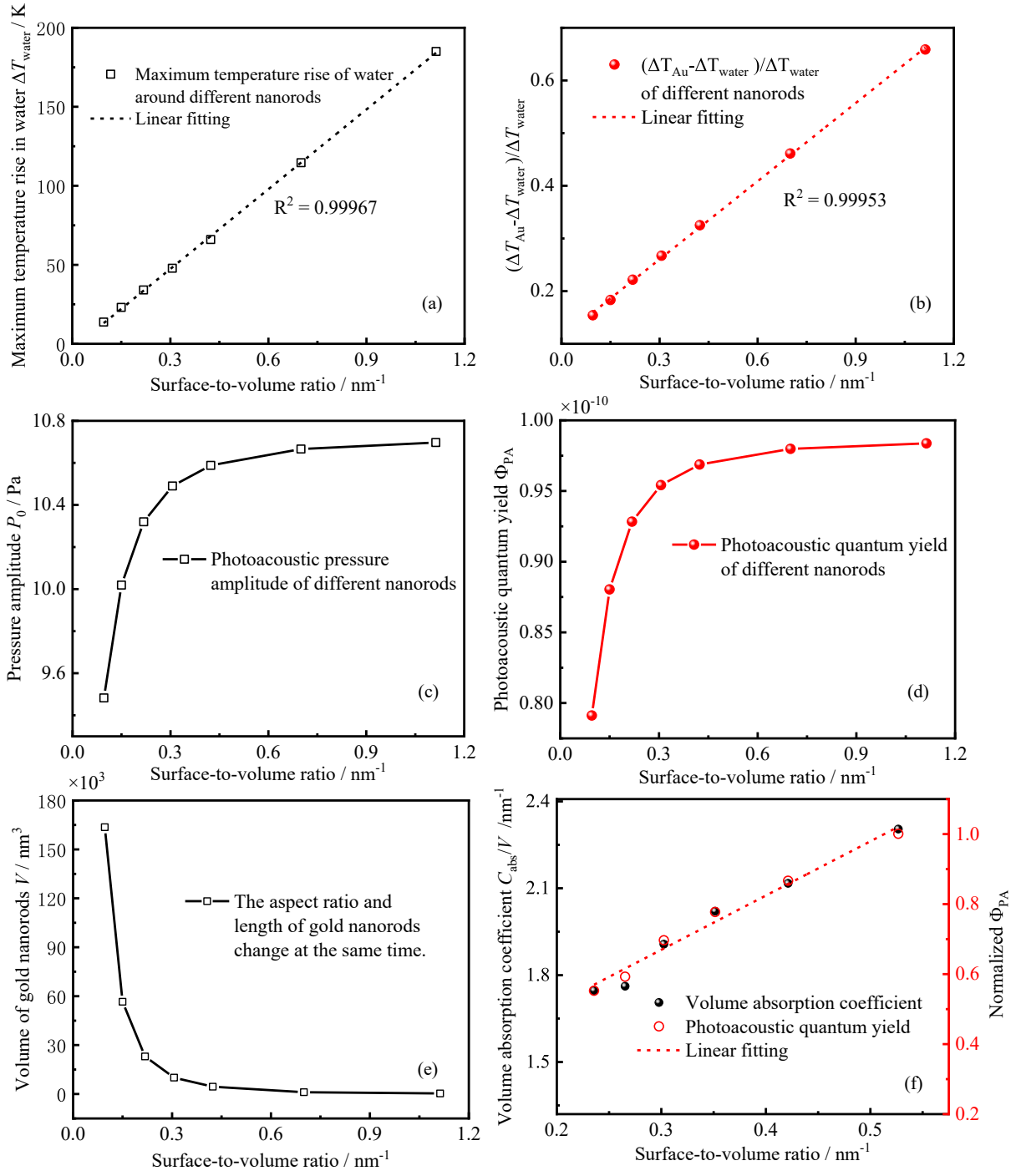

Fig. 6. Effects of specific surface area (surface-to-volume ratio) on photothermal and photoacoustic responses of single gold nanorods (the thermal energy obtained by a single gold nanorod is 50 fJ, and the pulse duration is 5 ns): (a) Variation of maximum temperature rise in water with specific surface area. (b) Variation of the ratio of the maximum temperature rise of gold nanorods to the maximum temperature rise in water with the specific surface area. (c) and (d) are the variations of photoacoustic pressure amplitude and photoacoustic quantum yield with specific surface area, respectively. (e) Variation of gold nanorod volume with specific surface area. (f) The results in Ref. [27]: there is a linear relationship between the photoacoustic efficiency of gold nanorods and the specific surface area. The results of volume absorption coefficient are calculated according to the data of Ref. [27].

solution through the study of the photoacoustic response of a single gold nanorod. Therefore, it is necessary to establish the relationship between the photoacoustic response of a single gold nanorod and the macro response. Here, the absorption of laser energy by water in the solution is ignored, and it is considered that the distance between gold nanorods is large enough to avoid the electromagnetic coupling and thermal coupling effects caused by the aggregation of gold nanorods. It should be emphasized that these assumptions are still achievable in biological tissues. Gold nanoparticles often require surface modification of biomolecules[50], such as PEG, for practical applications. These modifications are beneficial for increasing the half-life of particles in the circulation of the blood, targeting tumor, and should not have a significant effect on photoacoustic[51]. Biomolecules modified are highly charged and have polymeric properties can be effective stabilizers

through the introduction of colloidal stabilizers by using chemical coupling methods, electrostatic and physical adsorption[50]. In general, the concentration of gold nanorod solution is described by the mass of gold nanorod contained in unit volume of the solution. In order to study the effect of specific surface area of gold nanorods, for the same volume of solution containing different sizes of gold nanorods, gold nanorods should have the same total mass M and total thermal energy $E_{\text{total\_thermal}}$. Therefore, in the solution containing gold nanorods of different sizes, the corresponding single gold nanorods should contain the same thermal energy per unit volume, as shown in the following formula:

$$E_{\text{thermal}}/V_{\text{nanorod}} = E_{\text{total\_thermal}}\rho_{\text{Au}}/M = \text{const} \tag{13}$$

where, V_{nanorod} is the volume of a single gold nanorod.

When the propagation loss of photoacoustic pressure is ignored, the relationship between the photoacoustic pressure P generated by the gold nanorod solution and the photoacoustic pressure p generated by a single gold nanorod in the solution satisfies $P = Np$ [33] (N is the total number of gold nanorods in the solution), so the relationship between the total acoustic energy $E_{\text{total\_acoustic}}$ generated by the solution and the acoustic energy E_{acoustic} generated by a single gold nanorod can be described by the following formula:

$$E_{\text{total\_acoustic}} = \iint P^2 \Big/ \rho c \, \mathrm{d}S\mathrm{d}t = \iint (Np)^2 \Big/ \rho c \, \mathrm{d}S\mathrm{d}t = N^2 E_{\text{acoustic}} \tag{14}$$

Therefore, the relationship between the photoacoustic quantum yield $\Phi_{\text{total\_PA}}$ of gold nanorod solution and the photoacoustic quantum yield Φ_{PA} of single gold nanorod is satisfied:

$$\begin{aligned}\Phi_{\text{total\_PA}} &= \frac{E_{\text{total\_acoustic}}}{E_{\text{total\_thermal}}} = \frac{N^2 E_{\text{acoustic}}}{N E_{\text{thermal}}} = N\Phi_{\text{PA}} \\ &= \frac{M}{\rho_{\text{Au}}} \frac{\Phi_{\text{PA}}}{V_{\text{nanorod}}}\end{aligned} \tag{15}$$

It can be seen from the above formula that the photoacoustic quantum yield of gold nanorod solution is affected by the photoacoustic quantum yield and volume of a single gold nanorod at the same time. A mathematical model describing the relationship between photoacoustic quantum yield of gold nanorod solution with mass concentration and photoacoustic quantum yield of single gold nanorod has been established. In order to study the effect of specific surface area on the photoacoustic quantum yield of macroscopic solution described by mass concentration, from the established model, it can be known that for a single gold nanorod in solution, the heat source of gold nanorod of different size should meet the condition of fixed thermal energy per unit volume, seen in Eq. (13). The fixed value can be set as $E_{\text{thermal}}/V_{\text{nanorod}} = 0.1\ \text{J/m}^3$. Then, the maximum temperature rise and pressure amplitude of water medium around gold nanorods of different sizes with specific surface area were calculated, as shown in Fig. 7(a). It can be seen that both decrease with the increase of specific surface area, because the increase of specific surface area means that the volume of gold nanorods is smaller (as shown in Fig. 6(e)), the heat energy obtained by a single gold nanorod is reduced, and the maximum temperature rise and pressure amplitude of water are reduced. For the macro gold nanorod solution, when the mass concentration is the same, the number of gold nanorods in the gold nanorod solution with larger specific surface area is more and the total heat exchange area is larger. With the same total thermal energy obtained, although the maximum temperature rise of water decreases, the heat transfer capacity is stronger, and higher photoacoustic quantum yield can be obtained, as shown in Fig. 7(b). In addition, it should be declared that from Eq. (15), it can be seen that the photoacoustic quantum yield of gold nanorods described by mass density is related to the total mass and the volume of gold nanorods. For the sake of wide universality, we have normalized the photoacoustic quantum yield of macroscopic gold nanorod solution.

Oscar et al. [29] measured the maximum PA amplitude of the same four AuNRs in the A549 cells using an MSOT system at a fixed number of particles (1×10^{11} NP/ml) and fixed total mass (100 μg/ml). They got completely different results. At a fixed number density, AuNR-50 (the largest of the four sizes of gold nanorods) had the greatest photoacoustic pressure amplitude; In contrast, AuNR-10 (smallest volume) had the greatest photoacoustic pressure amplitude at a fixed mass concentration. Furthermore, when they tested the effect of gold nanorods size on cytotoxicity, it was observed that more total mass was taken up by the lung cancer cells compared with that of the smaller AuNRs. They speculated that the total number of particles may be a more important factor to consider for cellular uptake and targeting than total mass, which needed more detailed biological experiments to confirm this hypothesis. A cell is only going to uptake particles through endocytosis by a certain amount until they become toxic[52]. However, it is not clear whether this 'a certain amount' is a limit of number or a limit of mass, which determines the description of the concentration of gold nanoparticles in cells. Meanwhile, how to describe the concentration of gold nanorods is very important for predicting the photoacoustic response. Therefore, in addition to the mass of gold nanoparticles per unit volume, the

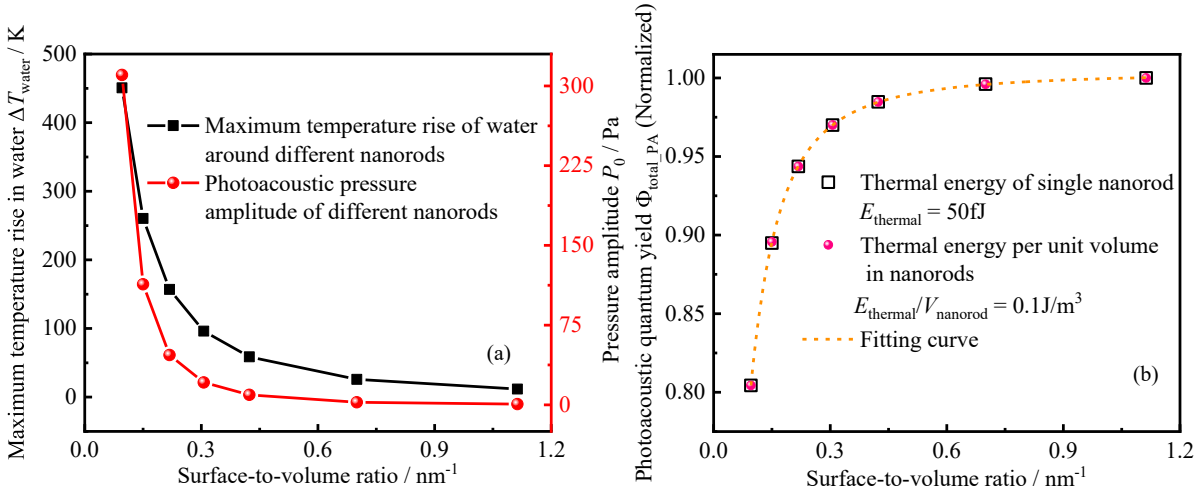

Fig. 7. Photothermal and photoacoustic responses of gold nanorods in mass concentration gold nanorod solution: (a) Variation of maximum temperature rise in water and pressure amplitude with specific surface area. The thermal energy per unit volume of gold nanorods is 0.1 J/m^3, and the pulse duration is 5 ns. (b) The normalized photoacoustic quantum yields of number density gold nanorod solution and mass concentration gold nanorod solution vary with specific surface area. The normalized results in the figure are obtained by dividing the calculation results of gold nanorods with AR = 8 and L = 30 nm.

concentration of gold nanoparticles described by the number density (i.e. the number of gold nanoparticles per unit volume) should be investigated. For the number density gold nanorod solution, in order to study the effect of specific surface area on the photoacoustic response of macro solution, different gold nanorod solutions should have the same number of gold nanorods N_{total} and the same total thermal energy under the same solution volume. Then, in the solution containing gold nanorods of different sizes, the thermal energy E_{thermal} obtained by a single gold nanorod satisfies:

$$E_{\text{thermal}} = E_{\text{total\_thermal}}/N_{\text{total}} = \text{const} \tag{16}$$

that is, in different sizes of gold nanorod solutions, the corresponding single gold nanorod should meet the same thermal energy obtained by a single particle. The photoacoustic quantum yield relationship between the solution and the corresponding single gold nanorod satisfies the following formula:

$$\Phi_{\text{total\_PA}} = \frac{E_{\text{total\_acoustic}}}{E_{\text{total\_thermal}}} = \frac{N^2 E_{\text{acoustic}}}{N E_{\text{thermal}}} = N_{\text{total}}\Phi_{\text{PA}} \tag{17}$$

This means that after the normalization of the analysis results in Fig. 6(d), the photoacoustic quantum yield of the number density gold nanorod solution with specific surface area can be obtained directly, as shown in Fig. 7(b). The results of normalized photoacoustic quantum yield of two concentrations of gold nanorod solutions (number density and mass concentration) were fitted, and it was found that the change curves of the two were almost the same. This shows that the photoacoustic quantum yield of gold nanorod solution changes the same with the specific surface area as long as the corresponding thermal energy conditions are met, regardless of the number density or mass concentration, which means that the photoacoustic quantum yield of the solution can get rid of the limitation of the concentration description method and well describe the influence of the specific surface area on its photoacoustic response.

Geometrical optimization of AuNRs

When gold nanorods are used as the contrast agent of photoacoustic imaging, it is expected to obtain a strong photoacoustic signal, which is conducive to improve the contrast of photoacoustic imaging. However, under the irradiation of specific wavelength pulsed laser, gold nanorods with different sizes show significant differences in photoacoustic response. This is because different sizes of gold nanorods show different absorption characteristics in a specific spectrum. At the same time, the change of size will also change the specific surface area of gold nanorods. Both of them will affect the photoacoustic response of gold nanorod solution. Therefore, it is necessary to comprehensively consider these two factors and optimize the size of gold nanorods at specific wavelengths to obtain the gold nanorod structure with the strongest photoacoustic response. According to the previous analysis, the photoacoustic quantum yield can describe the photoacoustic response of gold nanorod solution. In addition, the concentration of gold nanorod solution can be described by number density or mass concentration. When the number density is used to describe the concentration of gold nanorod solution, the relative magnitude of the absorption characteristics of gold nanorod solutions with different sizes with the same concentration can be expressed by the relative magnitude of the absorption cross section C_{abs} of a single gold nanorod. When the mass concentration is used to describe the gold nanorod solution, the relative magnitude of the absorption characteristics of different gold nanorod solutions can be described by the relative magnitude of the ratio of the absorption cross section of a single gold nanorod to the volume, which can be called the volume absorption coefficient [53], $\alpha = C_{\text{abs}}/V$. What's more, the size range of gold nanoparticles applied to biological tissues is also limited. The maximum size of gold nanoparticles should be less than 100 nm, otherwise the particle transmission through cell membrane will be affected, which may also cause additional problems [54,55]. The minimum size is limited by the current synthesis technology, that is, it is difficult to synthesize gold nanorods with small length and large aspect ratio. Therefore, the size range of gold nanorods optimized in this work is that the aspect ratio is 2–8, the length is 30–100 nm.

When gold nanorods are applied to the laser wavelength of 808 nm in the near-infrared region, in order to obtain the size of gold nanorods with the highest photoacoustic quantum yield, it is necessary to calculate the absorption characteristics of gold nanorods at this wavelength, as shown in Fig. 8(a) and Fig. 8(d). It can be seen that within the size range of gold nanorods studied, the absorption cross section and volume absorption coefficient of gold nanorods have the maximum values, but the sizes of gold nanorods corresponding to the maximum values of the two are obviously different. As mentioned earlier, the absorption cross section of gold nanorods is usually positively correlated with the volume. However, similar to gold nanospheres[56], when the volume of gold nanorods increases, the increasing rate of absorption cross section increases at first and then decreases. This means that when the size of gold nanorods changes, the volume absorption coefficient will have an extreme value[28]. Therefore, the distribution of absorption cross section C_{abs} and volume absorption cross section α with volume is significantly different, which leads to a significant difference in the size of gold nanorods corresponding to the maximum values of the two physical quantities. Then, the photoacoustic quantum yield of the corresponding solution can be calculated according to the absorption characteristics of gold nanorods. However, the amount of calculation is too large. The previous analysis shows that when the absorption characteristics and specific surface area of gold nanorods are quite different, the absorption characteristics will be the key factor determining the relative magnitude of photoacoustic quantum yield of gold nanorods. Therefore, when calculating the photoacoustic quantum yield of gold nanorods, only the size range of gold nanorods with high absorption characteristics needs to be paid attention to, as shown in Fig. 8(b) and Fig. 8(e). The calculation range of Fig. 8(b) and Fig. 8(e) is determined by the size parameters of gold nanorods with maximum absorption properties and the size parameter distribution with high absorption properties in Fig. 8(a) and Fig. 8(d). The selected range should fully show the size parameters of the absorption characteristics and photoacoustic quantum yield at the maximum, and reduce the amount of calculation as much as possible, which is the same situation for Fig. 8(c) and (f). On this basis, the photoacoustic quantum yield of the corresponding gold nanorod solution is calculated, as shown in Fig. 8(c) and Fig. 8(f). Fig. 8(b) and Fig. 8(e) are normalized to facilitate comparison with the photoacoustic quantum yield distribution of the corresponding gold nanorod solution. Moreover, Fig. 8(c) and Fig. 8(f) are also normalized because the absolute value of photoacoustic quantum yield of gold nanorod solution is strongly affected by pulsed laser fluence and solution concentration. The normalized results can eliminate the influence of these two factors, making the optimization results more universal reference value. From the comparison between Fig. 8(b)-(c) and Fig. 8(e)-(f), it can be seen that the photoacoustic quantum yield distribution of gold nanorod solution described by number density is highly similar to the absorption cross-section distribution, and the size of the gold nanorod solution has the maximum absorption characteristics, which is also completely consistent with the size of photoacoustic quantum yield. In contrast, the gold nanorod solution described by mass concentration has a distribution region of higher photoacoustic quantum yield, which shifts downward compared with the volume absorption coefficient. The reason is that when the concentration is the same, the relative magnitude of photoacoustic quantum yield of gold nanorod solution described by number density is directly proportional to the relative magnitude of photoacoustic quantum yield of single gold nanorod in the solution, as shown in Eq. (17). However, for the gold nanorod solution described by mass concentration, the relative magnitude of photoacoustic quantum yield is determined by the ratio of photoacoustic quantum yield and volume of a single gold nanorod, as shown in Eq. (15). Therefore, compared with

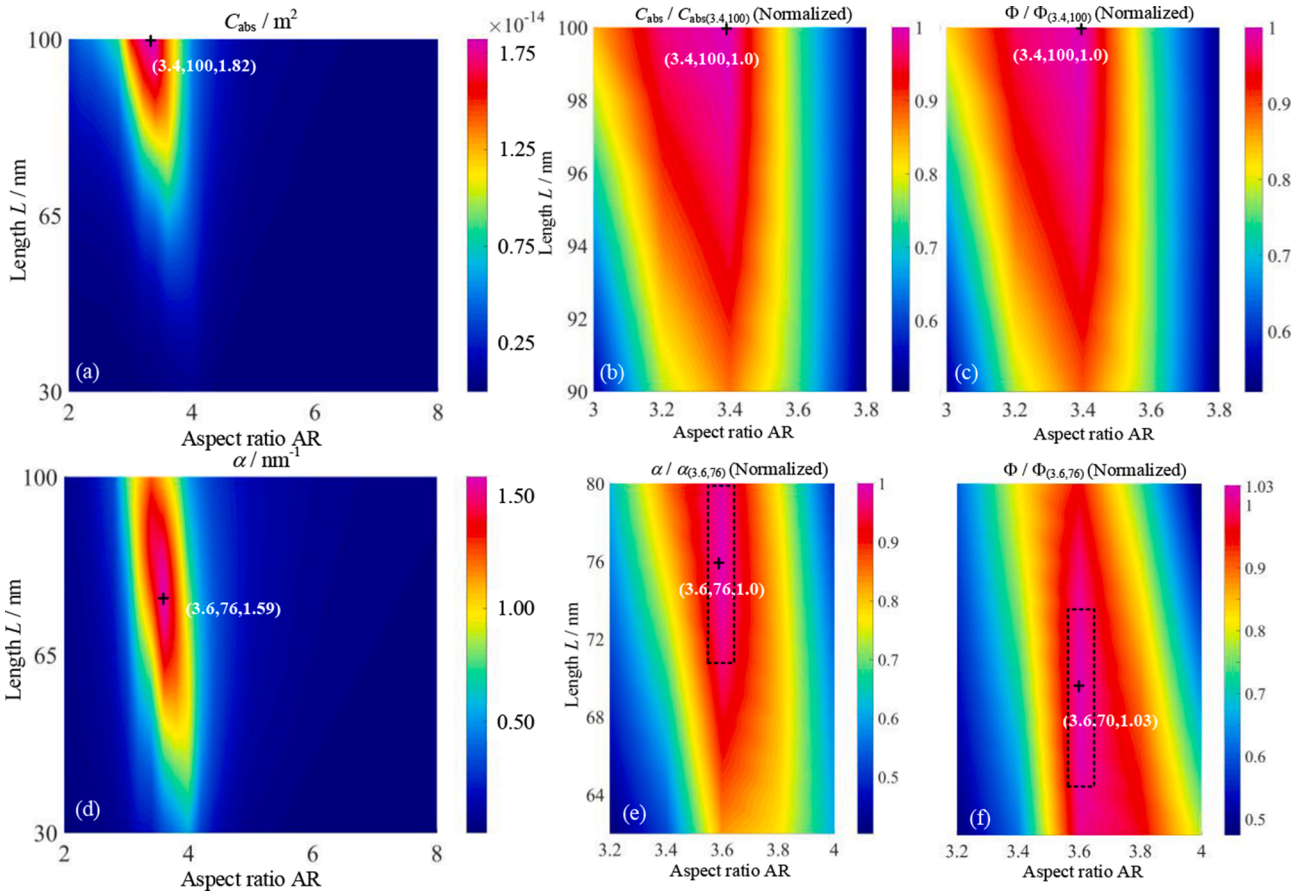

Fig. 8. Absorption characteristics and photoacoustic quantum of gold nanorods with different sizes at 808 nm: (a) and (d) are the absorption cross section and volume absorption coefficient distribution of gold nanorods at 808 nm wavelength, respectively. (b) and (c) are the normalized absorption cross section distribution and the normalized photoacoustic quantum yield distribution of number density gold nanorod solution, respectively, in the region of high absorption cross section. The normalized results in the figure are obtained by dividing the calculation results of gold nanorods with AR = 3.4 and L = 100 nm. (e) and (f) are the normalized volume absorption coefficient distribution and the normalized photoacoustic quantum yield distribution of mass concentration gold nanorod solution, respectively, in the region of high absorption cross section. The normalized results in the figure are obtained by dividing the calculation results of gold nanorods with AR = 3.6 and L = 70 nm. Fig. 8.(c) and (f) in the manuscript share the L scales with Fig. 8(b) and (e), respectively.

Fig. 8(e), the high photoacoustic quantum yield distribution region in Fig. 8(f) will shift to the smaller gold nanorod region.

Similarly, the size of gold nanorods was optimized for the other two laser wavelengths 895 nm and 1064 nm in the near-infrared region, as shown in Fig. 9. Comparing the results in Fig. 8 and Fig. 9, it can be found that the maximum absorption cross section of gold nanorods always occurs at the gold nanorods with a length of 100 nm (maximum length), which is consistent with the results observed in Fig. 4(a), and the maximum volume absorption coefficient will shift to the smaller gold nanorod region due to the influence of the volume of gold nanorods. Moreover, it can be observed that for the gold nanorod solution described by number density, the size of the gold nanorod corresponding to the maximum photoacoustic quantum yield is always consistent with that of the gold nanorod with the maximum absorption cross section. For the gold nanorod solution described by mass concentration, the size of the gold nanorod with the maximum photoacoustic quantum yield always shifts to the smaller gold nanorod region. However, it should be noted that for the gold nanorod solution described by mass concentration, although the size of the gold nanorod at the maximum volume absorption coefficient is inconsistent with that at the maximum photoacoustic quantum yield, there is no significant difference in the relative magnitude of the photoacoustic quantum yield of the gold nanorod solution corresponding to the two sizes (in this work, the maximum difference is no more than 3%). Therefore, in practical application, the size at the maximum volume absorption coefficient can be used to approximately replace the size at the maximum photoacoustic quantum yield. However, the difference in the size optimization results of gold nanorods caused by the difference of gold nanorod solution concentration description methods can not be ignored.

Near-infrared region is the transparent window of biological tissue, and the absorption rate of biological tissue in this region is very low. Therefore, high pulsed laser fluence is allowed to be used for photoacoustic imaging in the near-infrared region. The maximum permissible exposure limit for human skin at different wavelengths is 20 mJ/cm^2 at $400 < \lambda < 700$ nm, $20 \times 10^{0.002(\lambda-700)}$ mJ/cm^2 at $700 < \lambda < 1050$ nm and 100 mJ/cm^2 at $1050 < \lambda < 1500$ nm [16]. However, the thermal stability of gold nanorods is not ideal, that is, gold nanorods will melt and break under high pulse fluence. With the change of the morphology of gold nanorods, the absorption properties and photoacoustic response will be reduced. The melting and fragmentation mechanisms of gold nanorods are complex and their energy thresholds are different. Link et al.[57] found in experimental studies that the energy threshold for fragmentation with nanosecond pulses was around 1000 mJ/cm^{-2}, while ϕ-shaped gold nanoparticles were observed at 250 mJ/cm^{-2}. This means that in biological applications, the morphologic changes caused by the melting of gold nanorods are the main limitation of photostability. Molecular dynamics simulations show that the stability of gold nanorods is significantly affected by the energetics of its surface facets [58–60]. The gold surface roughens at about 680 K, the {1 0 0} surface disorders at about 1170 K, while the {1 1 1} surface remains stable up to

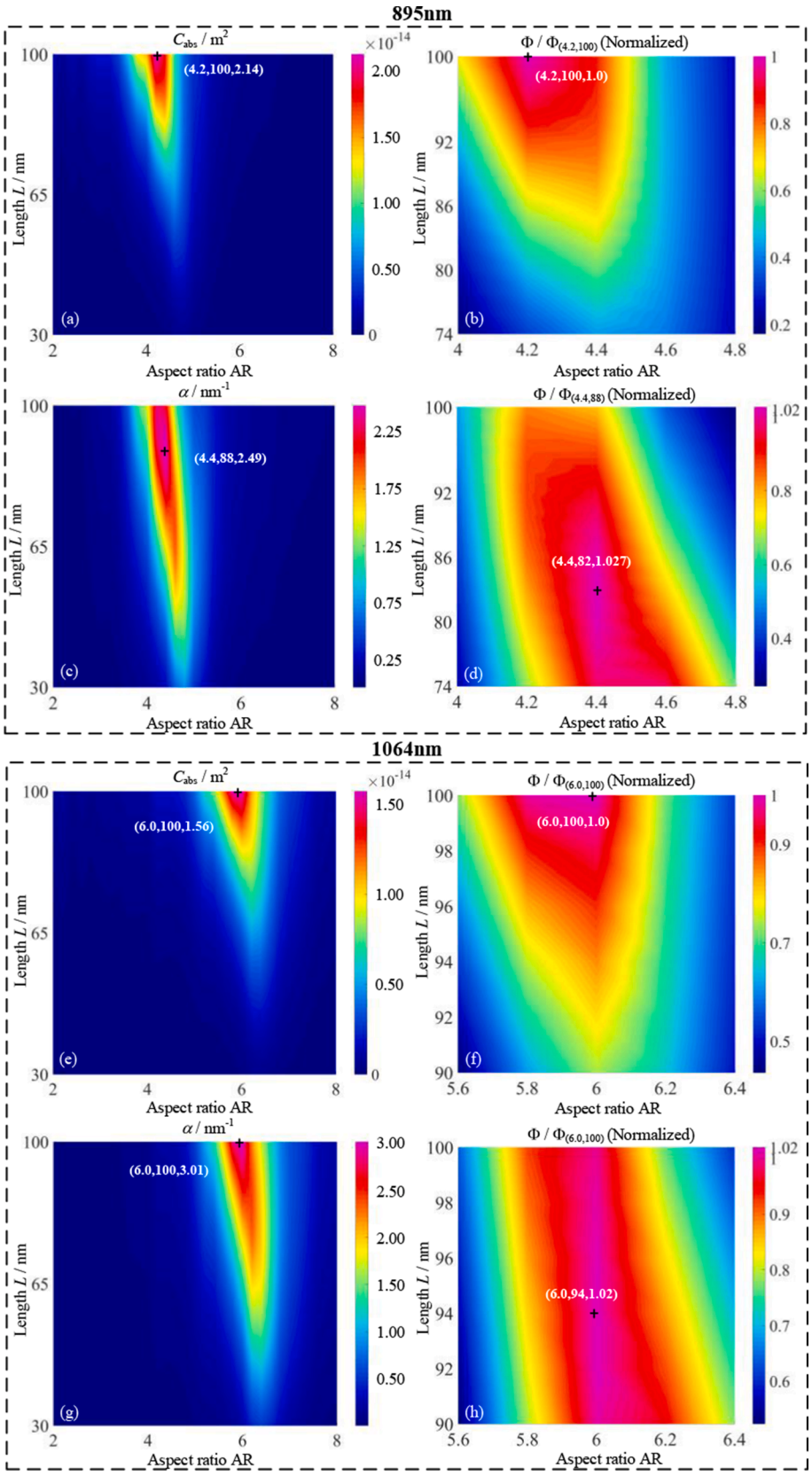

Fig. 9. Distribution of absorption characteristics and photoacoustic quantum yield of gold nanorods at 895 nm and 1064 nm: (a) and (e) are the absorption cross section distribution of gold nanorods at 895 nm and 1064 nm, respectively. (b) and (f) are the normalized photoacoustic quantum yield distributions of number density gold nanorod solutions at 895 nm and 1064 nm, respectively. (c) and (g) are the volume absorption coefficient distribution of gold nanorods at 895 nm and 1064 nm, respectively. (d) and (h) are the normalized photoacoustic quantum yield distributions of mass concentration gold nanorod solutions at 895 nm and 1064 nm, respectively.

the bulk melting point 1337 K[58]. At high temperature, {1 1 0} and {1 0 0} can change to {1 1 1} with the change of the morphology of gold nanorods. In addition, the surface melting temperature of gold nanorods is also affected by pulse duration[51]. When gold nanoparticles are irradiated by nanosecond pulse laser, the temperature increases rapidly and will transfer heat to water by thermal diffusion, resulting in a huge temperature gradient in water. The so-called boiling under very large temperature gradient is commonly related to the crossing of the spinodal

line, which occurs at a temperature (called spinodal temperature 550.15 K and different from the boiling point 373.15 K) just below the critical fluid temperature[61]. When the temperature of water reaches the node-turning temperature, the water around the gold nanorods will undergo gas–liquid phase change, and forms a bubble layer, which worsens the heat exchange environment of gold nanorods, so that the temperature of gold nanorods rises sharply[62,63]. With this high temperature process (gold nanorods typically reach temperatures of more than 1000 K), the gold nanorods are transformed into ϕ-shaped nanoparticles. Then, the absorption characteristics and photoacoustic response of gold nanorod solution are changed, and the utility of gold nanorod solution as contrast agent is reduced. Therefore, when gold nanorods are applied in the near-infrared region, the thermal stability of gold nanorods is also the key factor to improve their photoacoustic properties. According to the above analysis, the key to ensure the thermal stability of gold nanorods is to ensure that there is no phase transition in the surrounding aqueous medium, which means that the maximum temperature of water medium does not exceed the spinodal temperature when pulsed laser irradiates gold nanorods. The pulsed laser fluence when the water medium temperature around the gold nanorod reaches the spinodal temperature is defined as the critical phase transition fluence F_c. For the optimized gold nanorod sizes at 808 nm, 895 nm and 1064 nm in Fig. 8 and Fig. 9, the corresponding critical laser fluence is calculated, as shown in Table 3. It can be seen that the critical phase transition laser fluence of gold nanorods optimized at three wavelengths is smaller than that of critical safety laser fluence (F_c less than 10 mJ/cm^{-2}, while the maximum permissible exposure limit is more than 20 mJ/cm^{-2}). It means that in practical application, the pulse fluence of gold nanorods should be estimated by optical transmission simulation to avoid the reshaping of gold nanorods according to the critical phase change fluence. Moreover, the increase of the pulse duration of the pulsed laser t_w can significantly improve the critical phase transition laser fluence of gold nanorods. The reason is that the increase of the pulse duration of the pulsed laser t_w will significantly reduce the peak power density of laser, and then reduce the maximum temperature rise of gold nanorods and water, allowing gold nanorods to tolerate higher pulse laser fluence.

Table 3
Critical phase transition laser fluence of optimized gold nanorods at different pulse durations.

λ / nm	Size of gold nanorods	Critical phase transition laser fluence F_c / mJ•cm^{-2}			
		t_w = 2 ns	t_w = 5 ns	t_w = 10 ns	t_w = 20 ns
808	AR = 3.4 L = 100 nm	1.84	3.32	5.48	9.40
	AR = 3.6 L = 70 nm	2.04	4.00	6.88	12.32
895	AR = 4.2 L = 100 nm	1.32	2.44	4.08	7.08
	AR = 4.4 L = 82 nm	1.48	2.84	4.88	8.72
1064	AR = 6.0 L = 100 nm	1.32	2.60	4.44	7.92
	AR = 6.0 L = 94 nm	1.44	2.80	4.84	8.68

Conclusions

The size of the gold nanorod will affect its absorption across section and specific surface area at the same time, which will then affect its photothermal and photoacoustic responses. However, the weight of the specific surface area and absorption properties to change the photoacoustic response is not clear. In this work, the effects of these two factors on the photothermal and photoacoustic responses of gold nanorods were studied separately. The main conclusions are obtained as followed:

(1) The effect of interfacial thermal resistance G on the thermal coupling between gold nanorods of different sizes and water is different. There is a linear relationship between $(\Delta T_{Au} - \Delta T_{water})/\Delta T_{water}$ and specific surface area.
(2) For a single gold nanorod, compared with the effect of absorption cross section on photoacoustic quantum yield, the effect of specific surface area on photoacoustic quantum yield is not significant. The specific surface area of gold nanorods increased by 10.6 times, while the corresponding pressure amplitude and photoacoustic quantum yield increased by 0.13 times and 0.24 times respectively.
(3) For the gold nanorod solution, when the size of gold nanorods changes, the change of absorption characteristics (including absorption cross section and volume absorption cross section) will be the decisive factor for the dominant photoacoustic characteristics, and the specific surface area is the secondary factor, which can be ignored to a certain extent. The effect of specific surface area on photoacoustic quantum yield is less than 3%.
(4) The pulse laser with larger pulse duration should be selected, which is helpful to maintain the thermal stability of gold nanorods. When the pulse duration is 5 ns, the gold nanorods will melt under the pulse fluence of about 4 mJ/cm^2. However, when the pulse duration increases to 20 ns, the gold nanorods can withstand the pulse fluence of about 8 mJ/cm^2.

In this work, the background medium of gold nanorods' photoacoustic response is aqueous solution, which is significantly different from the optical properties of biological tissues. However, as the absorbance of gold nanoparticles is several orders of magnitude higher than that of these biomolecules, within the effective imaging depth of photoacoustic imaging, these photoacoustic signals will not strongly interfere with the photoacoustic signals produced by gold nanoparticles [16]. Therefore, the photoacoustic response of gold nanorods in aqueous solution is of reference value for that in biological tissues.

CRediT authorship contribution statement

Jian-Ping Sun: Conceptualization, Formal analysis, Methodology, Software, Validation, Visualization, Writing – original draft. **Ya-Tao Ren:** Conceptualization, Funding acquisition, Methodology, Supervision, Writing – review & editing. **Kai Wei:** Formal analysis, Investigation, Methodology, Visualization, Writing – review & editing. **Ming-Jian He:** Conceptualization, Formal analysis, Methodology, Writing – review & editing. **Bao-Hai Gao:** Formal analysis, Methodology, Validation, Writing – review & editing. **Hong Qi:** Conceptualization, Funding acquisition, Supervision, Writing – review & editing.

Declaration of Competing Interest

The authors declare that they have no known competing financial interests or personal relationships that could have appeared to influence the work reported in this paper.

Acknowledgements

This project has received funding from the National Natural Science Foundation of China (51806047), Natural Science Foundation of Heilongjiang Province (LH2019E047), Interdisciplinary Research Foundation of HIT (IR2021235), and the European Union's Horizon 2020 research and innovation programme under the Marie Skłodowska-Curie grant agreement No. 839641. The authors would like to thank Prof. Renxi Gao for the valuable discussion during the revision of this paper.

Availability of data and material

The data that support the plots within this paper and other findings of this study are available from the corresponding author upon reasonable request.

References

[1] Manohar S, Razansky D. Photoacoustics: a historical review. Adv. Opt. Photonics 2016;8(4):586. https://doi.org/10.1364/AOP.8.000586.
[2] Wilson K, Homan K, Emelianov S. Biomedical photoacoustics beyond thermal expansion using triggered nanodroplet vaporization for contrast-enhanced imaging. Nat. Commun. 2012;3:618.
[3] Liu YJ, Bhattarai P, Dai ZF, Chen XY. Photothermal therapy and photoacoustic imaging via nanotheranostics in fighting cancer. Chem. Soc. Rev. 2019;48:2053–108.
[4] Weber J, Beard PC, Bohndiek SE. Contrast agents for molecular photoacoustic imaging. Nat. Methods 2016;13:639–50.
[5] Nie LM, Chen XY. Structural and functional photoacoustic molecular tomography aided by emerging contrast agents. Chem. Soc. Rev. 2014;43:7132–70.
[6] Yguerabide J, Yguerabide EE. Light-scattering submicroscopic particles as highly fluorescent analogs and their use as tracer labels in clinical and biological applications - II. Experimental characterization. Anal. Biochem. 1998;262(2):157–76.
[7] Ren Y, Chen Q, He M, Zhang X, Qi H, Yan Y. Plasmonic Optical Tweezers for Particle Manipulation: Principles, Methods, and Applications. ACS Nano 2021;15(4):6105–28.
[8] Chang S-S, Shih C-W, Chen C-D, Lai W-C, Wang CRC. The shape transition of gold nanorods. Langmuir 1999;15(3):701–9.
[9] Lee KS, El-Sayed MA. Gold and silver nanoparticles in sensing and imaging: Sensitivity of plasmon response to size, shape, and metal composition. J. Phys. Chem. B 2006;110:19220–5.
[10] Mallidi S, Larson T, Tam J, Joshi PP, Karpiouk A, Sokolov K, et al. Multiwavelength Photoacoustic Imaging and Plasmon Resonance Coupling of Gold Nanoparticles for Selective Detection of Cancer. Nano Lett. 2009;9(8):2825–31.
[11] Kumar S, Aaron J, Sokolov K. Directional conjugation of antibodies to nanoparticles for synthesis of multiplexed optical contrast agents with both delivery and targeting moieties. Nat. Protoc. 2008;3(2):314–20.
[12] Song KH, Kim C, Cobley CM, Xia Y, Wang LV. Near-Infrared Gold Nanocages as a New Class of Tracers for Photoacoustic Sentinel Lymph Node Mapping on a Rat Model. Nano Lett. 2009;9(1):183–8.
[13] Kim J-W, Galanzha EI, Shashkov EV, Moon H-M, Zharov VP. Golden carbon nanotubes as multimodal photoacoustic and photothermal high-contrast molecular agents. Nat. Nanotechnol. 2009;4(10):688–94.
[14] Li M-L, Wang JC, Schwartz JA, Gill-Sharp KL, Stoica G, Wang LV. In-vivo photoacoustic microscopy of nanoshell extravasation from solid tumor vasculature. J. Biomed. Opt. 2009;14(1):010507. https://doi.org/10.1117/1.3081556.
[15] Kim C, Cho EC, Chen J, Song KH, Au L, Favazza C, et al. In Vivo Molecular Photoacoustic Tomography of Melanomas Targeted by Bioconjugated Gold Nanocages. ACS Nano 2010;4(8):4559–64.
[16] Li W, Chen X. Gold nanoparticles for photoacoustic imaging. Nanomedicine 2015;10(2):299–320.
[17] Chen Y-S, Frey W, Aglyamov S, Emelianov S. Environment-Dependent Generation of Photoacoustic Waves from Plasmonic Nanoparticles. Small 2012;8(1):47–52.
[18] Yu H-Q, Yao J, Wu X-W, Wu D-J, Liu X-J. Tunable photoacoustic properties of gold nanoshells with near-infrared optical responses. J. Appl. Phys. 2017;122(13):134901. https://doi.org/10.1063/1.4985860.
[19] Shahbazi K, Frey W, Chen Y-S, Aglyamov S, Emelianov S. Photoacoustics of core-shell nanospheres using comprehensive modeling and analytical solution approach. Commun. Phys.-UK 2019;2:119.
[20] Fukasawa T, Shinto H, Aoki H, Ito S, Ohshima M. Size-dependent effect of gold nanospheres on the acoustic pressure pulses from laser-irradiated suspensions. Adv. Powder Technol. 2014;25(2):733–8.
[21] Pang GA, Laufer J, Niessner R, Haisch C. Photoacoustic Signal Generation in Gold Nanospheres in Aqueous Solution: Signal Generation Enhancement and Particle Diameter Effects. J. Phys. Chem. C 2016;120:27646–56.
[22] Shinto H, Fukasawa T, Aoki H, Ito S, Ohshima M. Acoustic pressure pulses from laser-irradiated suspensions containing gold nanospheres in water: Experimental and theoretical study. Colloid Surf. A-Physicochem. Eng. Asp. 2013;430:51–7.
[23] Chen Q, Qi H, Ren YT, Sun JP, Ruan LM. Optical properties of truncated Au nanocages with different size and shape. AIP Adv. 2017;7:065115.
[24] Ren YT, Chen Q, Li HX, Qi H, Yan YY. Passive control of temperature distribution in cancerous tissue during photothermal therapy using optical phase change nanomaterials. Int. J. Therm. Sci. 2021;161:106754.
[25] He MJ, Qi H, Ren YT, Zhao YJ, Antezza M. Magnetoplasmonic manipulation of nanoscale thermal radiation using twisted graphene gratings. Int J Heat Mass Transf 2020;150:119305.
[26] Brioude A, Jiang XC, Pileni MP. Optical properties of gold nanorods: DDA simulations supported by experiments. J. Phys. Chem. B 2005;109:13138–42.
[27] Chen Y-S, Zhao Y, Yoon SJ, Gambhir SS, Emelianov S. Miniature gold nanorods for photoacoustic molecular imaging in the second near-infrared optical window. Nat. Nanotechnol. 2019;14(5):465–72.
[28] Shi Y, Yang S, Xing Da. Quantifying the Plasmonic Nanoparticle Size Effect on Photoacoustic Conversion Efficiency. J. Phys. Chem. C 2017;121(10):5805–11.
[29] Knights OB, Ye S, Ingram N, Freear S, McLaughlan JR. Optimising gold nanorods for photoacoustic imaging in vitro. Nanoscale Adv. 2019;1(4):1472–81.
[30] Song D, Jing D. Insight into the localized surface plasmon resonance property of core-satellite nanostructures: Theoretical prediction and experimental validation. J. Colloid Interface Sci. 2017;505:373–82.
[31] Cheng L, Zhu GX, Liu GN, Zhu LQ. FDTD simulation of the optical properties for gold nanoparticles. Mater. Res. Express 2020;7:125009.
[32] Oskooi AF, Roundy D, Ibanescu M, Bermel P, Joannopoulos JD, Johnson SG. MEEP: A flexible free-software package for electromagnetic simulations by the FDTD method. Comput. Phys. Commun. 2010;181:687–702.
[33] Gandolfi M, Banfi F, Glorieux C. Optical wavelength dependence of photoacoustic signal of gold nanofluid. Photoacoustics 2020;20:12.
[34] Hatef A, Darvish B, Sajjadi AY. Computational study of plasma-assisted photoacoustic response from gold nanoparticles irradiated by off-resonance ultrafast laser. J. Nanopart. Res. 2017;19:67.
[35] Govorov AO, Zhang W, Skeini T, Richardson H, Lee J, Kotov NA. Gold nanoparticle ensembles as heaters and actuators: melting and collective plasmon resonances. Nanoscale Res. Lett. 2006;1:84–90.
[36] Merabia S, Shenogin S, Joly L, Keblinski P, Barrat J-L. Heat transfer from nanoparticles: A corresponding state analysis. Proc. Natl. Acad. Sci. U. S. A. 2009;106(36):15113–8.
[37] Hatef A, Darvish B, Dagallier A, Davletshin YR, Johnston W, Kumaradas JC, et al. Analysis of Photoacoustic Response from Gold-Silver Alloy Nanoparticles Irradiated by Short Pulsed Laser in Water. J. Phys. Chem. C 2015;119:24075–80.
[38] Korenchenko AE, Beskachko VP. Determining the shear modulus of water in experiments with a floating disk. J. Appl. Mech. Tech. Phys. 2008;49:80–3.
[39] Gan RP, Fan HH, Wei ZC, Liu HY, Lan S, Dai QF. Photothermal Response of Hollow Gold Nanorods under Femtosecond Laser Irradiation. Nanomaterials 2019;9:711.
[40] Hoelen CGA, de Mul FFM. A new theoretical approach to photoacoustic signal generation. J. Acoust. Soc. Am. 1999;106:695–706.
[41] Ungureanu C, Rayavarapu RG, Manohar S, van Leeuwen TG. Discrete dipole approximation simulations of gold nanorod optical properties: Choice of input parameters and comparison with experiment. J. Appl. Phys. 2009;105(10):102032. https://doi.org/10.1063/1.3116139.
[42] Sharma SK, Shrivastava N, Rossi F, Tung LD, Thanh NTK. Nanoparticles-based magnetic and photo induced hyperthermia for cancer treatment. Nano Today 2019;29:100795. https://doi.org/10.1016/j.nantod.2019.100795.
[43] García-Álvarez R, Chen L, Nedilko A, Sánchez-Iglesias A, Rix A, Lederle W, et al. Optimizing the Geometry of Photoacoustically Active Gold Nanoparticles for Biomedical Imaging. ACS Photonics 2020;7(3):646–52.
[44] Cavigli L, Milanesi A, Khlebtsov BN, Centi S, Ratto F, Khlebtsov NG, et al. Impact of Kapitza resistance on the stability and efficiency of photoacoustic conversion from gold nanorods. J. Colloid Interface Sci. 2020;578:358–65.
[45] Moon H, Kumar D, Kim H, Sim C, Chang J-H, Kim J-M, et al. Amplified Photoacoustic Performance and Enhanced Photothermal Stability of Reduced Graphene Oxide Coated Gold Nanorods for Sensitive Photo acoustic Imaging. ACS Nano 2015;9(3):2711–9.
[46] Shi Y, Qin H, Yang S, Xing Da. Thermally confined shell coating amplifies the photoacoustic conversion efficiency of nanoprobes. Nano Res. 2016;9(12):3644–55.
[47] Nam SY, Ricles LM, Suggs LJ, Emelianov SY. Nonlinear photoacoustic signal increase from endocytosis of gold nanoparticles. Opt. Lett. 2012;37(22):4708. https://doi.org/10.1364/OL.37.004708.
[48] Shi Y, Cui D, Zhang Z. Quantitative Study of the Nonlinearly Enhanced Photoacoustic/Photothermal Effect by Strong LSPR-Coupled Nanoassemblies. Nanomaterials 2020;10(10):1942. https://doi.org/10.3390/nano10101942.
[49] Calasso IG, Craig W, Diebold GJ. Photoacoustic point source. Phys. Rev. Lett. 2001;86(16):3550–3.
[50] Aldewachi H, Chalati T, Woodroofe MN, Bricklebank N, Sharrack B, Gardiner P. Gold nanoparticle-based colorimetric biosensors. Nanoscale 2018;10(1):18–33.
[51] Cavigli L, Cini A, Centi S, Borri C, Lai S, Ratto F, et al. Photostability of Gold Nanorods upon Endosomal Confinement in Cultured Cells. J. Phys. Chem. C 2017;121(11):6393–400.
[52] Aaron J, Travis K, Harrison N, Sokolov K. Dynamic Imaging of Molecular Assemblies in Live Cells Based on Nanoparticle Plasmon Resonance Coupling. Nano Lett. 2009;9(10):3612–8.
[53] Tuersun P, Yakupu X, Han X, Yin Y. Optimization of Nonspherical Gold Nanoparticles for Photothermal Therapy. Appl. Sci.-Basel 2019;9(20):4300. https://doi.org/10.3390/app9204300.
[54] Chithrani BD, Ghazani AA, Chan WCW. Determining the size and shape dependence of gold nanoparticle uptake into mammalian cells. Nano Lett. 2006;6(4):662–8.
[55] Perrault SD, Walkey C, Jennings T, Fischer HC, Chan WCW. Mediating Tumor Targeting Efficiency of Nanoparticles Through Design. Nano Lett. 2009;9(5):1909–15.
[56] Metwally K, Mensah S, Baffou G. Fluence Threshold for Photothermal Bubble Generation Using Plasmonic Nanoparticles. J. Phys. Chem. C 2015;119(51):28586–96.
[57] Link S, Burda C, Nikoobakht B, El-Sayed MA. Laser-induced shape changes of colloidal gold nanorods using femtosecond and nanosecond laser pulses. J. Phys. Chem. B 2000;104(26):6152–63.
[58] Wang Y, Teitel S, Dellago C. Surface-driven bulk reorganization of gold nanorods. Nano Lett. 2005;5(11):2174–8.
[59] Qi WH, Wang MP. Size and shape dependent melting temperature of metallic nanoparticles. Mater Chem Phys 2004;88(2-3):280–4.

[60] Wang YT, Dellago C. Structural and morphological transitions in gold nanorods: A computer simulation study. J. Phys. Chem. B 2003;107:9214–9.
[61] Lombard J, Biben T, Merabia S. Nanobubbles around plasmonic nanoparticles: Thermodynamic analysis. Phys. Rev. E 2015;91(4). https://doi.org/10.1103/PhysRevE.91.043007.
[62] Karampelas IH, Liu K, Alali F, Furlani EP. Plasmonic Nanoframes for Photothermal Energy Conversion. J. Phys. Chem. C 2016;120(13):7256–64.
[63] Furlani EP, Karampelas IH, Xie Q. Analysis of pulsed laser plasmon-assisted photothermal heating and bubble generation at the nanoscale. Lab Chip 2012;12(19):3707. https://doi.org/10.1039/c2lc40495h.
[64] Johnson PB, Christy RW. Optical Constants of the Noble Metals. Phys. Rev. B 1972;6(12):4370–9.